

Electromagnetic Radial Diffusion in the Earth's Radiation Belts as Determined by the Solar Wind Immediate Time History and a Toy Model for the Electromagnetic Fields

Solène Lejosne¹

¹University of California, Berkeley

November 24, 2022

Abstract

Diffusion-driven radiation belt models require multiple physics-based inputs to specify the radiation environment through which spacecraft travel, including diffusion coefficients. Even though event-specific coefficients are necessary for model accuracy, their routine integration in operational models has not yet been achieved. In fact, one of the key inputs, the radial diffusion coefficient, is still commonly determined by a Kp-driven parameterization. This work presents a method to determine continuous time series of time-varying radial diffusion coefficients. A theoretical model is developed in which electromagnetic radial diffusion is controlled by the magnetopause immediate time history. Specifically, radial diffusion is described as a function of the average, variance, and autocorrelation time of the geocentric stand-off distance to the subsolar point on the magnetopause. Because the magnitudes of these three magnetopause parameters vary with time and magnetic activity, so does radial diffusion. To a lesser extent, radial diffusion is also controlled by the drift frequency of the radiation belt population. Moreover, radial diffusion is quantified using a standard model in which the magnetopause is controlled by the solar wind. Although the resulting diffusion coefficients span several orders of magnitude per Kp index, the median magnitudes are remarkably similar to the ones provided by the standard Kp-driven statistical parameterization.

1 **Electromagnetic Radial Diffusion in the Earth's Radiation Belts as Determined by the Solar**
2 **Wind Immediate Time History and a Toy Model for the Electromagnetic Fields**

3
4 Solène Lejosne¹

5 1. Space Science Laboratory, University of California, Berkeley

6 Corresponding author: S. Lejosne, solene@berkeley.edu

7
8
9 **Keywords**

10 Radial Diffusion – Radiation Belts – Solar Wind – Magnetopause – Turbulence

11
12
13 **Key points**

- 14 1. A model in which electromagnetic radial diffusion is determined by the immediate time
15 history of the magnetopause location is presented.
- 16 2. With the magnetopause controlled by the solar wind, the diffusion coefficients per Kp
17 index average similarly to the existing standard.
- 18 3. A time series of electromagnetic radial diffusion coefficients with a one-minute time
19 resolution is provided for the year 2013.

20 **Abstract**

21
22 Diffusion-driven radiation belt models require multiple physics-based inputs to specify the
23 radiation environment through which spacecraft travel, including diffusion coefficients. Even
24 though event-specific coefficients are necessary for model accuracy, their routine integration in
25 operational models has not yet been achieved. In fact, one of the key inputs, the radial diffusion
26 coefficient, is still commonly determined by a Kp -driven parameterization.

27 This work presents a method to determine continuous time series of time-varying radial diffusion
28 coefficients. A theoretical model is developed in which electromagnetic radial diffusion is
29 controlled by the magnetopause immediate time history. Specifically, radial diffusion is described
30 as a function of the average, variance, and autocorrelation time of the geocentric stand-off distance
31 to the subsolar point on the magnetopause. Because the magnitudes of these three magnetopause
32 parameters vary with time and magnetic activity, so does radial diffusion. To a lesser extent, radial
33 diffusion is also controlled by the drift frequency of the radiation belt population. Moreover, radial
34 diffusion is quantified using a standard model in which the magnetopause is controlled by the solar
35 wind. Although the resulting diffusion coefficients span several orders of magnitude per Kp index,
36 the median magnitudes are remarkably similar to the ones provided by the standard Kp -driven
37 statistical parameterization.

38
39

40 **Plain Language Summary**

41
42 An increasing number of spacecraft operate through or within the terrestrial radiation belts, a
43 region where charged energetic particles are trapped in the Earth's magnetic field. Computer codes
44 simulate this dynamic radiative environment, with the objective of improving spacecraft design
45 and understanding spacecraft anomalies. These codes are physics-based models. That is, they solve
46 a master diffusion equation using a series of inputs that summarize the effects of different physical
47 processes on particles. One of the key inputs to these codes is the radial diffusion coefficient. Yet
48 its formulation is currently limited: It is an average, obtained by interpolating a few experimental
49 data points, and the time resolution is no better than three hours. By detailing the physics
50 underlying radial diffusion in a simple scenario, this work provides a new quantification for the
51 radial diffusion coefficient. The time resolution is improved, and the coefficient variability is
52 enhanced. The fact that the resulting coefficient varies around the standard values provided by the
53 current reference adds credibility to the method. As a result, it is expected that this new
54 quantification will contribute to improving the accuracy of radiation belt simulations.

55 1. Introduction

56

57 Diffusion-driven radiation belt models have been developed and operated since the mid-1990s
 58 (Beutier & Boscher, 1995) to specify the structure, intensity and variability of the radiation
 59 environment through which satellites operate (e.g., Horne et al., 2013). They consist of solving a
 60 diffusion equation to describe radiation belt dynamics (e.g. Schulz & Lanzerotti, 1974), based on
 61 the adiabatic theory of magnetically trapped particles (e.g. Northrop, 1963). Operating a physics-
 62 based radiation belt model requires quantifying different inputs, including radial diffusion.

63

64 Radial diffusion is a statistical characterization of the violation of the third adiabatic invariant for
 65 a trapped radiation belt population. It plays a key role in determining radiation belt dynamics, not
 66 only at Earth but also at the giant planets (e.g., Lejosne & Kollmann, 2019).

67

68 The most commonly used radial diffusion inputs for terrestrial radiation belt models are the
 69 empirical coefficients for electromagnetic radial diffusion determined by Brautigam and Albert
 70 (2000), and parameterized by the Kp index:

71

$$\log_{10}(D_{LL}^{B\&A}/L^{10}) = -9.325 + 0.506 \times Kp [\log_{10}(\text{day}^{-1})] \quad (1)$$

72

73 where D_{LL} is the electromagnetic radial diffusion coefficient of a population of equatorial radiation
 74 belt particles, and the superscript “ $B\&A$ ” stands for Brautigam and Albert’s empirical law for radial
 75 diffusion. For non-equatorial particles of the same kinetic energy, the electromagnetic radial
 76 diffusion coefficient is proportional to the one in the equatorial case (Fälthammar, 1968; Schulz &
 77 Lanzerotti, 1974, p.89). Similar parameterization for equatorial electromagnetic radial diffusion
 78 was proposed by Ozeke et al. (2014) (Drozdov et al., 2017), based on the erroneous analytic
 79 expressions for radial diffusion developed by Fei et al. (2006) (Lejosne, 2019).

80

81 Brautigam and Albert’s empirical law for electromagnetic radial diffusion presents advantageous
 82 features for operational models (e.g., Glauert et al., 2018). First, radiation belt simulations yield
 83 plausible results when using such formulation for radial diffusion (e.g., Kim et al., 2011). Second,
 84 the implementation of the formula is straightforward. Moreover, it provides uninterrupted (i.e.,
 85 operational) evaluation of radial diffusion. On the other hand, even though the importance of using
 86 event-specific inputs to improve model accuracy is now recognized (e.g., Tu et al., 2009), their
 87 determination is seemingly incompatible with operational models. Indeed, the development of
 88 event-specific coefficients has called for intensive work so far: It requires running potentially
 89 costly numerical simulations (e.g., Li Z. et al., 2017), and/or carrying detailed analysis of specific
 90 data sets when available (e.g., Ali et al., 2016). Even so, uncertainty in the magnitude of these
 91 tailored, “event-specific” radial diffusion coefficients leads to uncertainty in the relative
 92 contribution of other processes to the observed particle distribution (e.g., Mann et al., 2016; Shprits
 93 et al., 2018; Mann et al., 2018). Such features hamper our ability to include event-specific radial
 94 diffusion coefficients in operational radiation belt models.

95
 96 The objective of this work is to provide a method to build operational, event-specific,
 97 electromagnetic diffusion coefficients. It builds on the theoretical framework underlying
 98 Brautigam and Albert (2000)'s empirical formula for electromagnetic radial diffusion. The
 99 theoretical model is detailed in **Section 2**, together with its reformulation in terms of fluctuations
 100 of the magnetopause location. Applying Shue et al. (1998)'s magnetopause model, the magnitude
 101 and variability of the resulting radial diffusion coefficients are discussed in **Section 3**. **Section 4**
 102 presents the results in the case of the year 2013, together with a comparison with the
 103 electromagnetic radial diffusion coefficients estimated according to Brautigam and Albert (2000)'s
 104 formula. The approach is discussed **Section 5**.

105
 106

107 **2. Theoretical Model Description**

108

109 **2.1. Theoretical Framework Associated with Brautigam and Albert (2000)'s Formula for** 110 **Electromagnetic Radial Diffusion**

111

112 Brautigam and Albert (2000)'s empirical formula for electromagnetic radial diffusion is a least
 113 squares interpolation of experimental values obtained at $L = 4$ by Lanzerotti and Morgan (1973)
 114 and at $L = 6.6$ by Lanzerotti et al. (1978). In both cases, a time interval of one week to one month
 115 of magnetic field fluctuations was analyzed to quantify an analytic expression for electromagnetic
 116 radial diffusion. The analytic expression, developed by Fälthammar (1965; 1968), and further
 117 detailed by Schulz and Eviatar (1969), is the following:

118

$$\frac{D_{LL}}{L^{10}} = \frac{\Omega^2}{8} \left(\frac{5}{7}\right)^2 \frac{R_E^2}{B_E^2} P_A(\Omega) \quad (2)$$

119

120 for equatorially mirroring particles, where $B_E \cong 0.3 G$ is the magnetic equatorial field at the Earth
 121 surface, $R_E \cong 6400 km$ is one Earth radius, $\Omega/2\pi$ is the trapped population drift frequency, and
 122 P_A is the power spectrum of the asymmetric field fluctuations of a simplified electromagnetic field
 123 model.

124

125 The magnetic field model is a magnetic dipole field to which a small perturbation is superimposed
 126 (Mead, 1964). The small perturbation is the sum of two components: a symmetric component,
 127 $S(t)$, independent of local time, φ , and an asymmetric component, $A(t)rcos\varphi$. An additional
 128 assumption connects both symmetric and asymmetric components of the magnetic field
 129 perturbation to the magnetopause location:

130

$$S(t) = \frac{B_1}{\ell^3(t)} \quad (3)$$

131
132 and
133

$$A(t) = \frac{-B_2}{R_E \ell^4(t)} \quad (4)$$

134
135 where $B_1 \cong 0.25 G$ and $B_2 \cong 0.21 G$, and $\ell \sim 10 R_E$ is the geocentric stand-off distance to the
136 subsolar point on the magnetopause, normalized in units of Earth Radii (e.g., Schulz & Eviatar,
137 1969). As a result, the power spectrum of the asymmetric field fluctuations is proportional to the
138 power spectrum of the symmetric field fluctuations, and the **equation (2)** for electromagnetic
139 radial diffusion is also:
140

$$\frac{D_{LL}}{L^{10}} = 2\Omega^2 \left(\frac{5B_2}{21B_1B_E} \right)^2 \frac{1}{\ell^2} P_S(\Omega) \quad (5)$$

141
142 Because a fluctuation of the magnetopause location, ℓ' , leads to a symmetric fluctuation of the
143 magnetic field, S' , that is about 10 times greater than the asymmetric one, A' , ($A'R_E =$
144 $-4B_2S'/(3B_1\ell) \sim -0.1S'$), $P_S(\Omega)$ is more readily measurable than $P_A(\Omega)$. That is why the
145 **equation (5)** is usually preferred to the **equation (2)** when it comes to evaluating radial diffusion
146 experimentally (Lanzerotti & Morgan, 1973; Lanzerotti et al., 1978).
147

148 Alternatively, one can also reformulate **equation (2)** in terms of fluctuations in the magnetopause
149 location since the magnitude of the magnetic field asymmetry is directly related to the
150 magnetopause location (**equation (4)**).
151

152 **2.2. Theoretical Model for Electromagnetic Radial Diffusion as Determined by the** 153 **Magnetopause Location**

154
155 Combining **equations (2) and (4)** yields:
156

$$\frac{D_{LL}}{L^{10}} = \frac{\Omega^2}{2} \left(\frac{20}{7} \right)^2 \left(\frac{B_2}{B_E} \right)^2 \frac{1}{\bar{\ell}^{10}} \int_0^\infty \overline{\ell'(0)\ell'(u)} \cos(\Omega u) du \quad (6)$$

157
158 where $\bar{\ell}$ is the average magnetopause location, $\ell' = \ell - \bar{\ell}$ is the fluctuating part of the
159 magnetopause location, and $(u \mapsto \overline{\ell'(0)\ell'(u)})$ is the autocorrelation function of the

160 magnetopause location. Further assuming that the autocorrelation function of the magnetopause
 161 location is subject to an exponential decay:
 162

$$\overline{\mathcal{B}'(0)\mathcal{B}'(u)} = \overline{\mathcal{B}'^2} e^{-u/\tau} \quad (7)$$

163
 164 where τ is the fluctuation lifetime, and $\overline{\mathcal{B}'^2}$ is the variance of the signal. It results that:
 165

$$\frac{D_{LL}}{L^{10}} = \frac{1}{2} \left(\frac{20}{7}\right)^2 \left(\frac{B_2}{B_E}\right)^2 \frac{\overline{\mathcal{B}'^2}}{\overline{\mathcal{B}}^{10}} \frac{\Omega^2 \tau}{1 + \Omega^2 \tau^2} \quad (8)$$

166
 167 Because radial diffusion coefficients are usually expressed on a logarithmic scale, let us focus on
 168 $\log_{10}(D_{LL}/L^{10})$ in the remainder of the article:
 169

$$\log_{10}(D_{LL}/L^{10}) = -10\log_{10}(\overline{\mathcal{B}}) + \log_{10}(\overline{\mathcal{B}'^2}) + \log_{10}\left(\frac{\Omega^2 \tau}{1 + \Omega^2 \tau^2}\right) + C \quad (9)$$

170
 171 where
 172

$$C = \log_{10}\left(\frac{1}{2}\left(\frac{20}{7}\right)^2 \left(\frac{B_2}{B_E}\right)^2\right) \cong 0.3 \quad (10)$$

173
 174 is a constant. The third term on the right-hand side of **equation (9)** is the only term that explicitly
 175 depends on the kinetic energy of the trapped population. It reaches a maximum equal to $-\log_{10}\tau$
 176 at very high energies, when $\Omega\tau \gg 1$. On the other hand, assuming that the fluctuation lifetime is
 177 very small in comparison with the radiation belt population drift period ($\Omega\tau \ll 1$), **equation (9)**
 178 becomes:
 179

$$\log_{10}(D_{LL}/L^{10}) = F(\overline{\mathcal{B}}; \overline{\mathcal{B}'^2}; \tau) + 2\log_{10}\Omega + C \quad (11)$$

180
 181 where
 182

$$F(\overline{\mathcal{B}}; \overline{\mathcal{B}'^2}; \tau) = -10\log_{10}(\overline{\mathcal{B}}) + \log_{10}(\overline{\mathcal{B}'^2}) + \log_{10}(\tau) \quad (12)$$

183

184 is a function controlled by the statistical characteristics of the magnetopause location.

185
 186 In any case, one needs to evaluate the average magnetopause location, $\bar{\ell}$, the variance of the
 187 magnetopause location, $\overline{\ell'^2}$, and the lifetime of the magnetopause fluctuations, τ , in order to
 188 quantify electromagnetic radial diffusion. Shue et al. (1998)'s magnetopause model provides a fast
 189 and accessible way to evaluate of these magnetopause parameters. In this model, the stand-off
 190 distance to the magnetopause is controlled by the dynamic pressure of the solar wind, and the
 191 orientation of the interplanetary magnetic field (IMF):

$$\ell = (10.22 + 1.29 \tanh(0.184 \times (B_z + 8.14))) D_p^{-1/6.6} \quad (13)$$

193
 194 where the solar wind dynamic pressure, D_p , is in nanopascals, and the north-south component of
 195 the IMF, B_z , is in nanoteslas (Shue et al., 1998). This model will be used in the following in order
 196 to quantify radial diffusion.

197
 198

199 3. Quantification

200 3.1. Origin of Radial Diffusion Time Variability

201
 202 In **equation (2)**, and thus in **equations (6)-(12)**, $A(t)$, and thus $\ell(t)$, are considered to be
 203 realizations of a stationary stochastic process. In other words, it is assumed that the magnetopause
 204 location fluctuates randomly and that its statistical properties are time-independent. In practice,
 205 the signal $\ell(t)$ does not correspond to realizations of a strictly stationary process, and the
 206 statistical properties of ℓ are time varying. Thus, it is necessary to specify a sample window size
 207 to evaluate the statistical characteristics of the magnetopause location. As a result, **equation (11)**
 208 becomes:

209

$$\log_{10}(D_{LL}/L^{10}) = F_T + 2\log_{10}\Omega + C \quad (14)$$

210
 211 where

212

$$F_T = -10\log_{10}(\bar{\ell}_T) + \log_{10}(\overline{\ell'^2}_T) + \log_{10}(\tau_T) \quad (15)$$

213
 214 and the subscript indicates that the quantity depends on the window size chosen, T . The moving
 215 average of the magnetopause location is:

216

$$\bar{\ell}_T = \frac{1}{T} \int_{-T/2}^{T/2} \ell(u) du \quad (16)$$

217

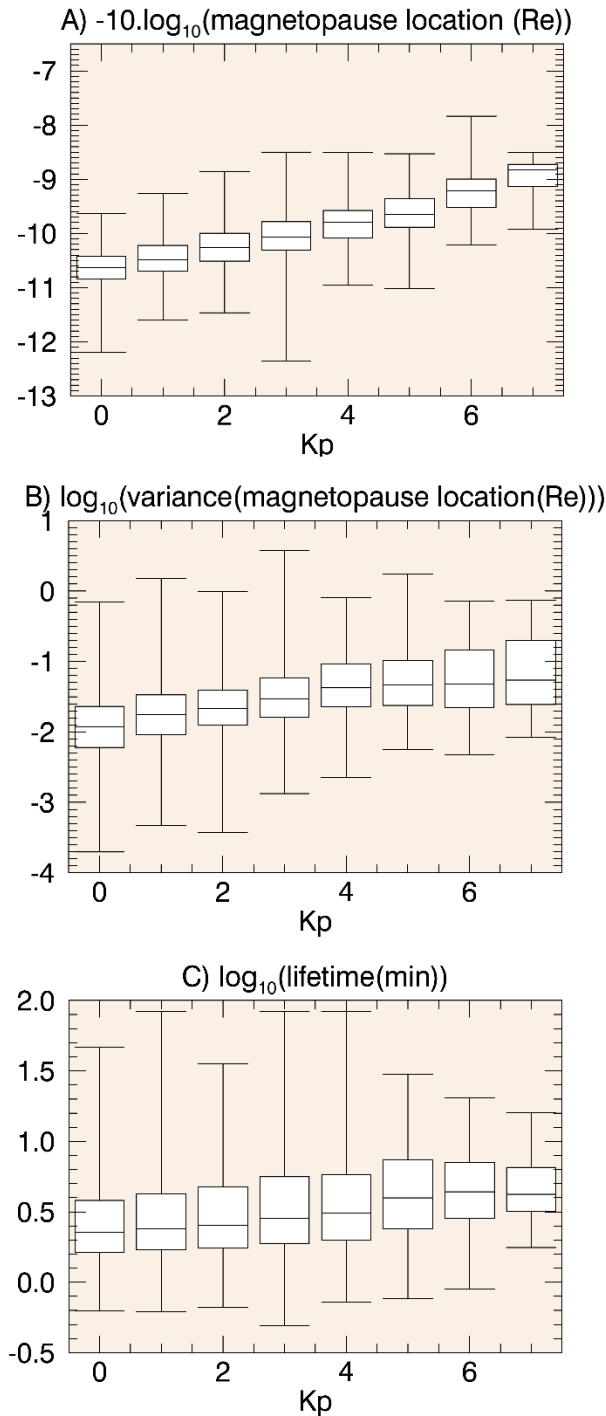
218 and the moving variance of the magnetopause location is:

219

$$\overline{\ell'^2}_T = \frac{1}{T} \int^T (\ell(u) - \bar{\ell}_T(u))^2 du \quad (17)$$

220

221 Thus, the time variability of the electromagnetic radial diffusion coefficient comes from the time
 222 variability of the statistical characteristics of the magnetopause location (average, variance, and
 223 lifetime). The radial diffusion coefficient increases 1) when the magnetopause average location
 224 decreases, 2) when the magnetopause fluctuations increase, or 3) when the lifetime increases
 225 (**equations (14)-(15)**). Which of these three possible effects has the most control over radial
 226 diffusion variability? In particular, why does the radial diffusion coefficient increase with Kp ? To
 227 investigate this question, the three components of F_T were computed for the year 2013 with a one-
 228 hour window size ($T = 1h$). To pilot the magnetopause location (**equation (13)**) solar wind inputs
 229 with a one-min time resolution were extracted from NASA/GSFC's OMNI data set through
 230 OMNIWeb (<https://omniweb.gsfc.nasa.gov/>). The average and the variance were computed
 231 according to **equation (16)** and **(17)**, respectively, and the lifetime τ was determined by fitting the
 232 autocorrelation function to an exponential decay. The results are summarized by boxplots
 233 parameterized by the Kp index and they are presented **Figure 1**.



234
 235 **Figure 1:** Magnitude of the three radial diffusion components that depend on the statistical
 236 characteristics of the magnetopause location, A) $-10 \log_{10}(\bar{r})$, B) $\log_{10}(\overline{r'^2})$, and C) $\log_{10}(\tau)$
 237 (see text for definitions). The ends of the whiskers correspond to the minimum and maximum
 238 values, the bottoms and the tops of the boxes are the lower and upper quartiles, and the bands
 239 inside the boxes are the medians. The sample window size chosen for the computations is one hour
 240 ($T = 1h$).

241

242 The **Figure 1** suggests that the magnitude of radial diffusion increases with the Kp index both
243 because the average magnetopause location decreases with Kp (**Fig. 1A**) and because the
244 fluctuations in magnetopause location increase with Kp (**Fig. 1B**). On the other hand, the
245 fluctuation lifetime does not seem to depend much on Kp (**Fig. 1C**). It is typically of the order of
246 a few minutes (< 10 min). Thus, for particles with drift periods that are such that $\Omega < 5$ mHz, i.e.,
247 for radiation belt particles below a few MeV (e.g. Schulz and Lanzerotti, 1974, p.13), the
248 assumption $\Omega\tau \ll 1$ is typically valid, and the **equation (11)** is a good approximation of the
249 **equation (10)**.

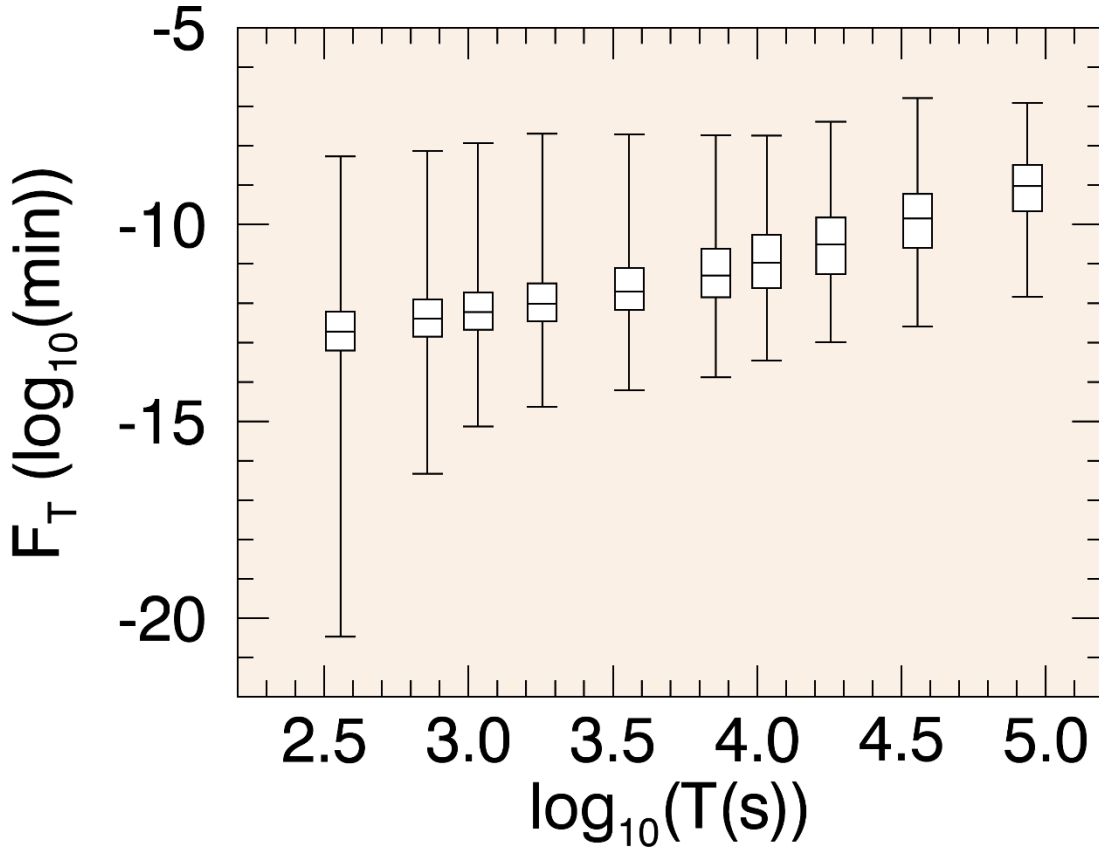
250

251 **3.2. Effect of the Sample Window Size on the Quantification of Radial Diffusion**

252

253 The statistical characteristics of the magnetopause location presented **Figure 1** were determined
254 using a sample window of one hour ($T = 1h$). To what extent does the choice of a sample window
255 size affect the statistical characteristics of the magnetopause location, as summarized by F_T , thus,
256 the magnitude of radial diffusion? To investigate this question, the function F_T was computed for
257 10 different sample window sizes over the year 2013: $T =$
258 $[6 \text{ min}, 12 \text{ min}, 18 \text{ min}, 30 \text{ min}, 1 \text{ h}, 2 \text{ h}, 3 \text{ h}, 5 \text{ h}, 10 \text{ h}, 24 \text{ h}]$. The results are summarized by
259 boxplots, and they are displayed **Figure 2**.

260



261 **Figure 2:** Magnitude of the parameter, F_T , which quantifies the effect of statistical characteristics
 262 of the magnetopause location on radial diffusion, as a function of the sample window size chosen
 263 for the statistical computations, T . The ends of the whiskers indicate the minimum and maximum
 264 values, the bottoms and the tops of the boxes are the lower and upper quartiles, and the bands
 265 inside the boxes are the medians.
 266

267 The **Figure 2** shows that the magnitude of F_T decreases as the window size, T , decreases. This is
 268 because the average magnetopause location fits better the instantaneous value of the magnetopause
 269 location as the window size T decreases. Thus, the variance decreases as the window size decreases
 270 ($\overline{\delta'^2} = 0$ for the asymptotic case in which $T=0$). A linear interpolation of F_T as a function of
 271 $\log_{10}(T)$ yields that, on average:
 272
 273

$$\frac{dF_T}{d(\log_{10}(T))} \cong 1.5 \quad (18)$$

274 with a standard deviation of 0.4.
 275

276
 277 When the objective is to quantify radial diffusion, the selected window size, T , must be consistent
 278 with the adiabatic invariant theory of magnetically trapped particles. Indeed, field fluctuations that
 279 evolve on timescales longer than the trapped population drift period conserve the third adiabatic
 280 invariant. On the other hand, asymmetric field fluctuations with characteristic times comprised
 281 between the bounce and the drift period violate the third invariant, driving radial diffusion (e.g.,
 282 Northrop, 1963). Thus, the window size, T , must be such that all field fluctuations that are on
 283 timescales longer than the drift period are stored in $\bar{\mathcal{L}}$ while field fluctuations that are between the
 284 bounce and the drift period are in \mathcal{L}' . Given the one-minute time resolution of the input signal, the
 285 characteristic time for the variation of the field is always greater than the bounce period.
 286 Nonetheless, the window size, T , needs to be long in comparison with the trapped population drift
 287 period in order to compute the average, $\bar{\mathcal{L}}$:
 288

$$T = \frac{2\pi k}{\Omega} \quad (19)$$

289
 290 where k is a constant greater than one: $k > 1$. As a result, F_T is in fact dependent on the trapped
 291 population drift frequency. Indeed, combining **equations (18)** and **(19)** yields:
 292

$$\frac{d F_T}{d(\log_{10}(\Omega))} \cong -1.5 \quad (20)$$

293
 294 As the kinetic energy increases, the drift frequency increases, thus, the magnitude of F_T decreases.
 295 In other words, the particle's drift motion is less and less sensitive to field fluctuations as the drift
 296 velocity increases (the discrepancies between $\bar{\mathcal{L}}$ and $\mathcal{L}(t)$ decrease as the drift period - thus T -
 297 decreases). Therefore, one should ideally tailor the computation of **equation (9)** according to the
 298 drift frequency. Yet, the expected dependence of radial diffusion on drift frequency is relatively
 299 weak. Indeed, for $\Omega\tau \ll 1$, combining **equation (20)** and **equation (14)** yields
 300

$$d(\log_{10}(D_{LL}/L^{10}))/d(\log_{10}(\Omega)) \cong 0.5 \quad (21)$$

301
 302 Thus, the magnitude of radial diffusion D_{LL} increases by about a factor 3 when the drift frequency
 303 increases by a factor 10. In comparison, for $\Omega\tau \gg 1$, assuming that the drift frequency dependence
 304 of F_T comes primarily from the variance, i.e., $dF/d(\log_{10}(\Omega)) \approx d(\log_{10}(\overline{\mathcal{L}'^2}))/d(\log_{10}(\Omega))$:
 305

$$d(\log_{10}(D_{LL}/L^{10}))/d(\log_{10}(\Omega)) \cong -1.5 < 0 \quad (22)$$

306
 307 Thus, there is a cutoff in radial diffusion efficiency once the drift period becomes smaller than the
 308 fluctuation lifetime. Assuming that the order of magnitude obtained **equation (22)** is valid, the
 309 magnitude of radial diffusion D_{LL} decreases by about a factor 30 when the drift frequency increases
 310 by a factor 10.

311
 312 While the selected window size needs to be consistent with adiabatic invariant theory, it also needs
 313 to be consistent with the mathematical assumptions underlying the model. In particular, field
 314 fluctuations must be regarded as realizations of a stationary process within the time interval
 315 considered. Such conditions are most likely achieved during magnetically quiet times, and/or when
 316 considering a relatively small time interval. Since the latter is not necessarily consistent with
 317 **equation (19)**, this poses a problem to radial diffusion quantification.

318
 319 In the following, it is proposed to work with a sample window size of one hour: $T_{1h} = 1 h$. A one-
 320 hour window is small enough to render radial diffusion variability with magnetic activity (as
 321 illustrated **Figure 1**) and to expedite the computations. It is also large enough to maintain sufficient
 322 data points to perform the required statistical analyzes. The average proportional relationship
 323 between the function, F_T , and the logarithmic of the drift frequency, $\log_{10}(\Omega)$, is used to evaluate
 324 the appropriate value of F_T from F_{1h} . Combining **equations (14)**, **(19)** and **(20)** yields:

$$\log_{10}(D_{LL}/L^{10}) = F_{1h} + 1.5 \log_{10}(2\pi k/T_{1h}) + 0.5 \log_{10}(\Omega) + C \quad (23)$$

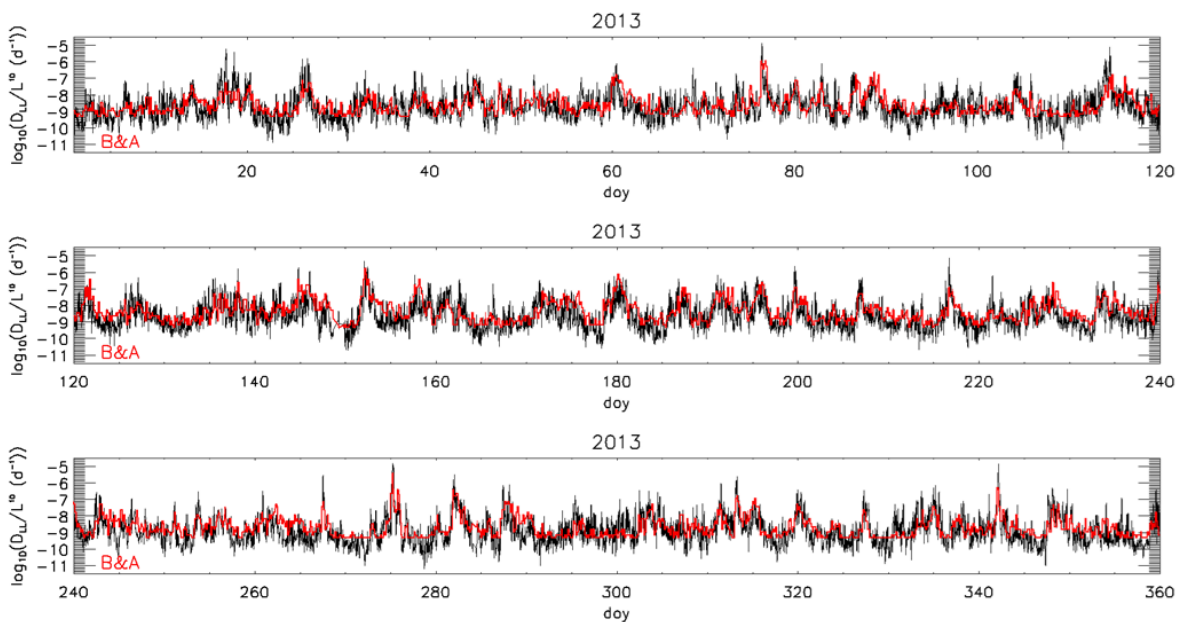
326
 327 for $\Omega < 5 mHz$. Given the uncertainty in hands, the choice of the constant $k > 1$ is unimportant.
 328 It is set to $k = 10$ in the remainder. The radial diffusion coefficient is usually in $[day^{-1}]$ while
 329 the angular drift velocity is usually in $[mHz]$. As a result, a reformulation of the **equation (23)** is:

$$\log_{10}(D_{LL}/L^{10}) = F_{1h} + 0.5 \log_{10}(\Omega) + 2.9 \quad (24)$$

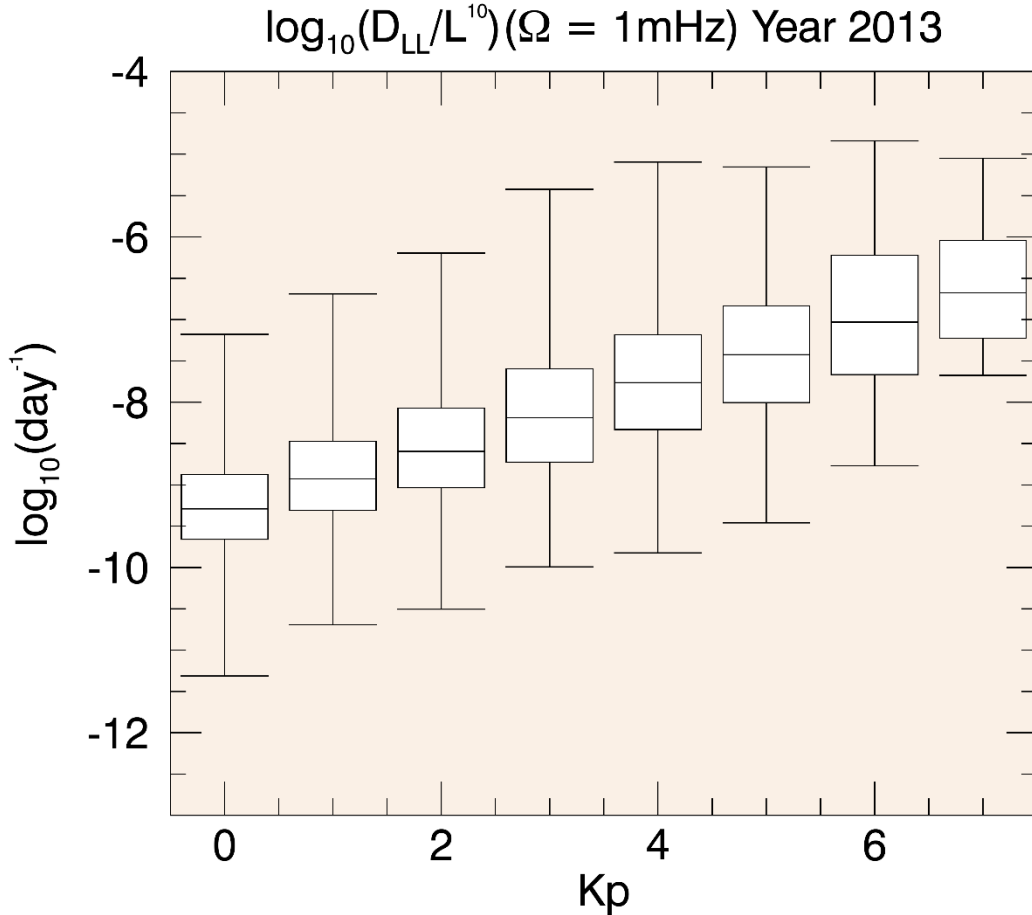
331
 332 where D_{LL} is evaluated in $[day^{-1}]$, F_{1h} is provided in $[\log_{10}(min)]$, and Ω is in $[mHz]$.

333
 334
 335 **4. Results and Comparison with Brautigam and Albert's Empirical Formula**
 336
 337 The radial diffusion coefficients were computed for the year 2013 for a radiation belt population
 338 of angular drift velocity $\Omega = 1 mHz$, following **equation (24)**. The time series is represented in

339 the **Figure 3** and it is compared to Brautigam and Albert’s estimates for electromagnetic radial
 340 diffusion. The comparison highlights a) the overall good agreement between the two times series,
 341 b) the greater variability of the radial diffusion coefficients determined by the solar wind
 342 immediate time history, and c) some limitations of the statistical model. For instance, Brautigam
 343 and Albert’s empirical formula has a lower threshold of $\log_{10}(D_{LL}/L^{10}) = -9.325$ during quiet
 344 times ($Kp = 0$). The existence of a lower threshold for radial diffusion is not physical, since there
 345 would be no radial diffusion (i.e., $D_{LL} = 0$) if the electromagnetic fields were perfectly stationary.
 346 On the other hand, the radial diffusion coefficients determined by the solar wind immediate time
 347 history can be smaller, in accordance with theoretical expectations. The results were also binned
 348 according to the Kp index, and they are summarized in boxplots displayed **Figure 4**.
 349



350
 351 **Figure 3.** Electromagnetic radial diffusion as a function of the day of the year (doy) in 2013. The
 352 radial diffusion coefficients determined as a function of the solar wind immediate time history are
 353 in black. The radial diffusion coefficients determined by Brautigam and Albert (2000)’s empirical
 354 formula (B&A) are in red.
 355



356
 357 **Figure 4.** Statistical characterization of the electromagnetic radial diffusion magnitude for the year
 358 2013, as a function of the Kp index, for a population of angular drift velocity $\Omega = 1 \text{ mHz}$. The
 359 ends of the whiskers indicate the minimum and maximum values, the bottoms and the tops of the
 360 boxes are the lower and upper quartiles, and the bands inside the boxes are the medians. The values
 361 were computed for the year 2013 according to **equation (24)**, with a one-minute time resolution.

362
 363 A linear interpolation of the medians per Kp index for the electromagnetic radial diffusion
 364 magnitude yields:

$$\log_{10}(D_{LL}/L^{10}) = -9.309 + 0.377 \times Kp \text{ [log}_{10}(\text{day}^{-1})] \quad (25)$$

366
 367 This interpolation is remarkably similar to the one obtained by Brautigam and Albert (2000)
 368 (**equation (1)**). The difference in the intercepts is $< 1\%$ while the slope as a function of Kp is only
 369 25% smaller than the one found by Brautigam and Albert. One reason for such similarity may be
 370 that both estimates rely on the same theoretical toy model for the electromagnetic fields. Yet, the

371 radial diffusion coefficients obtained by Lanzerotti and Morgan (1973) and Lanzerotti et al. (1978)
 372 were based on an analysis of magnetic field fluctuations measured by at ground level (at $L=4$) and
 373 at synchronous equatorial altitude ($L=6.6$). In these analyzes, the power spectrum of the
 374 fluctuations was fitted to a functional form ($P \propto \Omega^{-s}$, with s between 1 and 3). On the other hand,
 375 the numerical evaluations proposed here rely on solar wind measurements, and the autocorrelation
 376 function is fitted to an exponential decay (**equation (7)**). Because τ is found to be very small, both
 377 fitting methods are usually equivalent: In both cases, the power spectrum decreases as $\propto \Omega^{-2}$ over
 378 a large frequency range.

379 The time series of the three parameters constitutive of F_{1h} together with the magnitude of
 380 $\log_{10}(D_{LL}/L^{10})$ computed for the year 2013 for a radiation belt population of angular drift
 381 frequency $\Omega = 1 \text{ mHz}$ is accessible online (<http://doi.org/10.5281/zenodo.3625265>).

382

383

384 5. Discussion

385

386 The pros and cons of the method developed in this paper are summarized in the following.

387

388 First, the method faces the same theoretical limitations as the ones underlying Brautigam and
 389 Albert's formula for electromagnetic diffusion. Namely: It relies on an oversimplified
 390 electromagnetic field model (a "toy model"). Even when fitting the simplified Mead (1964)'s
 391 magnetic field formula to a basic external magnetic field model, such as the one developed by
 392 Tsyganenko (1989), discrepancies appear. There is also little doubt that the response of the
 393 magnetospheric fields to fluctuations in the magnetopause location is more complicated than what
 394 is actually described by the theoretical picture provided here. The proposed radial diffusion
 395 coefficients are also limited at both high and low L values. Indeed, at high L values, the
 396 electromagnetic field is expected to be more distorted and more variable than predicted. In that
 397 context, the distinction between L and L^* is also necessary (e.g. Roederer & Lejosne, 2018). At
 398 low L values, electrostatic radial diffusion is probably very important (e.g., O'Brien et al., 2016;
 399 Selesnick et al., 2016), and yet such diffusion process is not taken into account here.

400

401 Even so, the resulting coefficients binned as a function of the Kp index display remarkable
 402 agreement an empirical law that is generally considered standard. Furthermore, the theoretical
 403 picture presented here provides physical insights on the origin of radial diffusion variability: radial
 404 diffusion increases as the Kp index increases both because the magnetic field is more compressed
 405 (thus, the average asymmetry increases), and because it fluctuates more (thus, the variance of the
 406 asymmetry increases). The model also describes how electromagnetic radial diffusion varies with
 407 drift frequency. When the drift frequency increases, the part of the radial diffusion coefficient that
 408 explicitly depends on energy (third term **equation (9)**) increases, until it plateaus (for $\Omega\tau \gg 1$).
 409 The term that quantifies the effect of the statistical characteristics of the magnetopause, F_T , is also
 410 indirectly controlled by drift frequency. Indeed, the signal decomposition into an average and a
 411 fluctuating part requires the definition of a reference. The reference, set by adiabatic invariant
 412 theory, is the drift period. Field variations that evolve on time scales greater than the drift period
 413 are part of the average (that is, they do not violate the third invariant), while field variations that

414 evolve on time scales shorter than the drift period constitute the fluctuating part of the signal. As
 415 the drift frequency increases, the average describes more and more precisely the signal
 416 instantaneous values, and the variance decreases. Thus, F_T decreases as the drift frequency
 417 increases. As a result, there is a sweet spot in drift frequency at which radial diffusion is maximal,
 418 Ω_{max} . A derivation of **equation (9)** with respect to $\log_{10}(\Omega)$ yields $\Omega_{max} \approx 0.6/\tau$. With a
 419 fluctuation lifetime, τ , of the order of a couple of minutes, $\Omega_{max} \approx 5$ mHz. Even so, for $\Omega\tau \ll 1$,
 420 as is typically the case for most radiation belt particles, the resulting dependence of
 421 electromagnetic radial diffusion on drift frequency is relatively weak ($D_{LL} \propto \sim \Omega^{0.5}$). Such feature
 422 greatly simplifies radial diffusion quantification.

423 In the most general case, radial diffusion is controlled by the asymmetry in the electromagnetic
 424 field fluctuations (e.g., Northrop, 1963; Lejosne et al., 2012). Thus, quantifying radial diffusion
 425 requires monitoring electromagnetic field fluctuations. While previous work attempted to monitor
 426 the asymmetry of the magnetic field at geostationary orbit (Lejosne et al., 2013), this new model
 427 presents the advantage of being operational. Leveraging a toy model for the fields, the asymmetry
 428 of the field is controlled by the magnetopause, whose location is a function of solar wind
 429 parameters. Interestingly enough, it is not the first time that the solar wind is chosen to drive radial
 430 diffusion (Li et al., 2001). From a technical standpoint, the advantage of working with such a
 431 simple model is that it highlights some of the challenges that need to be addressed to quantify
 432 radial diffusion accurately, regardless of the model complexity. In particular, this work highlights
 433 some of the difficulties related to the analysis of non-stationary field fluctuations.

434

435

436

437 **Acknowledgments**

438

439 The work of S.L. was performed under JHU/APL Contract No. 922613 (RBSP-EFW) and NASA
 440 Grant Award 80NSSC18K1223. The use of NASA/GSFC's Space Physics Data Facility's
 441 OMNIWeb (<https://omniweb.gsfc.nasa.gov/>) service and OMNI data is acknowledged.

442 **References**

- 443
- 444 Ali, A. F., Malaspina, D. M., Elkington, S. R., Jaynes, A. N., Chan, A. A., Wygant, J., and Kletzing,
445 C. A. (2016), Electric and magnetic radial diffusion coefficients using the Van Allen probes data,
446 J. Geophys. Res. Space Physics, 121, 9586– 9607, doi:10.1002/2016JA023002.
- 447
- 448 Beutier, T., and Boscher, D. (1995), A three-dimensional analysis of the electron radiation belt by
449 the Salammbô code, J. Geophys. Res., 100(A8), 14853– 14861, doi:10.1029/94JA03066.
- 450
- 451 Brautigam, D.H., Albert, J.M. (2000), Radial diffusion analysis of outer radiation belt electrons
452 during the October 9, 1990, magnetic storm. J. Geophys. Res., 105(A1), 291–309.
453 <https://doi.org/10.1029/1999JA900344>
- 454
- 455 Drozdov, A. Y., Shprits, Y. Y., Aseev, N. A., Kellerman, A. C., and Reeves, G. D. (2017),
456 Dependence of radiation belt simulations to assumed radial diffusion rates tested for two empirical
457 models of radial transport, Space Weather, 15, 150– 162, doi:10.1002/2016SW001426.
- 458
- 459 Fälthammar, C.-G. (1965), Effects of time-dependent electric fields on geomagnetically trapped
460 radiation. J. Geophys. Res., 70(11), 2503–2516. <https://doi.org/10.1029/JZ070i011p02503>
- 461
- 462 Fälthammar, C.-G. (1968), Radial diffusion by violation of the third adiabatic invariant, in Earth's
463 Particles and Fields, edited by B. M. McCormac, pp. 157–169, Reinhold, New York.
- 464
- 465 Fei, Y., Chan, A.A., Elkington, S.R., & Wiltberger, M. J. (2006). Radial diffusion and MHD
466 particle simulations of relativistic electron transport by ULF waves in the September 1998 storm,
467 J. Geophys. Res., 111, A12209, doi:10.1029/2005JA011211.
- 468
- 469 Glauert, S. A., Horne, R. B., & Meredith, N. P. (2018). A 30-year simulation of the outer electron
470 radiation belt. Space Weather, 16, 1498– 1522. <https://doi.org/10.1029/2018SW001981>
- 471
- 472 Horne, R. B., Glauert, S. A., Meredith, N. P., Boscher, D., Maget, V., Heynderickx, D., and
473 Pitchford, D. (2013), Space weather impacts on satellites and forecasting the Earth's electron
474 radiation belts with SPACECAST, Space Weather, 11, 169– 186, doi:10.1002/swe.20023.
- 475
- 476 Kim, K.-C., Shprits, Y., Subbotin, D., and Ni, B. (2011), Understanding the dynamic evolution of
477 the relativistic electron slot region including radial and pitch angle diffusion, J. Geophys. Res.,
478 116, A10214, doi:10.1029/2011JA016684.
- 479
- 480 Lanzerotti, L. J., & Morgan, C. G. (1973). ULF geomagnetic power near L = 4: 2. Temporal
481 variation of the radial diffusion coefficient for relativistic electrons, J. Geophys. Res., 78(22),
482 4600–4610, doi:10.1029/JA078i022p04600.
- 483

- 484 Lanzerotti, L. J., Webb, D. C., & Arthur, C. W. (1978). Geomagnetic field fluctuations at
485 synchronous orbit 2. Radial diffusion, J. Geophys. Res., 83(A8), 3866–3870,
486 doi:10.1029/JA083iA08p03866.
- 487
- 488 Lejosne, S., Boscher, D., Maget, V., and Rolland, G. (2012), Bounce-averaged approach to radial
489 diffusion modeling: From a new derivation of the instantaneous rate of change of the third
490 adiabatic invariant to the characterization of the radial diffusion process, J. Geophys. Res., 117,
491 A08231, doi:10.1029/2012JA018011.
- 492
- 493 Lejosne, S., Boscher, D., Maget, V., and Rolland, G. (2013), Deriving electromagnetic radial
494 diffusion coefficients of radiation belt equatorial particles for different levels of magnetic activity
495 based on magnetic field measurements at geostationary orbit, J. Geophys. Res. Space Physics, 118,
496 3147– 3156, doi:10.1002/jgra.50361.
- 497
- 498 Lejosne, S. (2019). Analytic expressions for radial diffusion. Journal of Geophysical Research:
499 Space Physics, 124, 4278– 4294. <https://doi.org/10.1029/2019JA026786>
- 500
- 501 Lejosne, S., and Kollmann, P. (2019), Radiation Belt Radial Diffusion at Earth and Beyond. Earth
502 and Space Science Open Archive. <https://doi.org/10.1002/essoar.10501074.1>
- 503
- 504 Li, X., Temerin, M., Baker, D.N., Reeves, G.D., and Larson, D., (2001), Quantitative prediction
505 of radiation belt electrons at geostationary orbit based on solar wind measurements, Geophys. Res.
506 Lett., 28 (9), 1887-1890. <https://doi.org/10.1029/2000GL012681>
- 507
- 508 Li, Z., Hudson, M., Patel, M., Wiltberger, M., Boyd, A., and Turner, D. (2017), ULF wave analysis
509 and radial diffusion calculation using a global MHD model for the 17 March 2013 and 2015
510 storms, J. Geophys. Res. Space Physics, 122, 7353– 7363, doi:10.1002/2016JA023846.
- 511
- 512 Mann, I.R., et al. (2016), Explaining the dynamics of the ultra-relativistic third Van Allen radiation
513 belt. Nature Phys. 12:978–983. <https://doi.org/10.1038/nphys3799> 3154 3155
- 514
- 515 Mann, I.R., et al. (2018). Reply to ‘The dynamics of Van Allen belts revisited’. Nature Physics,
516 14(2), 103–104. <https://doi.org/10.1038/nphys4351>
- 517
- 518 Mead, G. D. (1964). Deformation of the geomagnetic field by the solar wind, J. Geophys. Res.,
519 69(7), 1181– 1195, doi:10.1029/JZ069i007p01181.
- 520
- 521 Northrop, T.G. (1963), *The Adiabatic Motion of Charged Particles*. Wiley Interscience, Hoboken,
522 N. J. ISBN-13: 978-0470651391.
- 523
- 524 O'Brien, T. P., Claudepierre, S. G., Guild, T. B., Fennell, J. F., Turner, D. L., Blake, J. B.,
525 Clemmons, J. H., and Roeder, J. L. (2016), Inner zone and slot electron radial diffusion revisited,
526 Geophys. Res. Lett., 43, 7301– 7310, doi:10.1002/2016GL069749.

- 527
528 Ozeke, L. G., Mann, I. R., Murphy, K. R., Jonathan Rae, I., and Milling, D. K. (2014), Analytic
529 expressions for ULF wave radiation belt radial diffusion coefficients, *J. Geophys. Res. Space*
530 *Physics*, 119, 1587– 1605, doi:10.1002/2013JA019204.
- 531
532 Roederer, J. G., & Lejosne, S. (2018). Coordinates for representing radiation belt particle flux. *J.*
533 *Geophys. Res. Space Physics*, 123, 1381– 1387. <https://doi.org/10.1002/2017JA025053>
- 534
535 Schulz, M., and Eviatar, A. (1969), Diffusion of equatorial particles in the outer radiation zone, *J.*
536 *Geophys. Res.*, 74(9), 2182– 2192, doi:10.1029/JA074i009p02182.
- 537
538 Schulz, M. and Lanzerotti, L.J. (1974), *Particle Diffusion in the Radiation Belts*. Springer-Verlag
539 Berlin Heidelberg. <https://doi.org/10.1007/978-3-642-65675-0>
- 540
541 Selesnick, R. S., Su, Y.-J., and Blake, J. B. (2016), Control of the innermost electron radiation belt
542 by large-scale electric fields, *J. Geophys. Res. Space Physics*, 121, 8417– 8427,
543 doi:10.1002/2016JA022973.
- 544
545 Shprits Y.Y., et al. (2018), The dynamics of Van Allen belts revisited. *Nature Physics*, 14, 102–
546 103. <https://doi.org/10.1038/nphys4350>
- 547
548 Shue, J.-H., et al. (1998), Magnetopause location under extreme solar wind conditions, *J. Geophys.*
549 *Res.*, 103(A8), 17691– 17700, doi:10.1029/98JA01103.
- 550
551 Tsyganenko, N. A. (1989), A magnetospheric magnetic field model with a warped tail current
552 sheet, *Planet. Space Sci.*, 37(1), 5–20.
- 553
554 Tu, W., Li, X., Chen, Y., Reeves, G. D., and Temerin, M. (2009), Storm-dependent radiation belt
555 electron dynamics, *J. Geophys. Res.*, 114, A02217, doi:10.1029/2008JA013480